HHS Public Access

Author manuscript

Biomaterials. Author manuscript; available in PMC 2019 March 01.

Published in final edited form as:

Biomaterials. 2018 March ; 157: 76–85. doi:10.1016/j.biomaterials.2017.11.044.

Influence of Diabetes on the Foreign Body Response to Nitric Oxide-Releasing Implants

Robert J. Soto[†], **Elizabeth P. Merricks**[‡], **Dwight A. Bellinger**[‡], **Timothy C. Nichols**[‡], and **Mark H. Schoenfisch**[†,*]

[†]Department of Chemistry, University of North Carolina, Chapel Hill, NC 27599, United States

[‡]Departments of Pathology and Laboratory Medicine, University of North Carolina, Chapel Hill, NC 27599, United States

Abstract

The foreign body response (FBR) to nitric oxide (NO)-releasing subcutaneous implants was compared between healthy and streptozotocin-induced diabetic swine by evaluating inflammation, collagen capsule formation, and angiogenesis. Steel wire substrates were first modified with polyurethane membranes capable of diverse NO-release kinetics (NO fluxes and release durations of 0.8–630.0 pmol cm^{-2} s^{-1} and 2–13 d, respectively). The NO-releasing materials were implanted in the subcutis for 3, 10, or 25 d for histological and immunohistochemical evaluation of the FBR. A delayed, more severe inflammatory response to control (i.e., non-NO-releasing) implants was observed in diabetic pigs relative to healthy swine. Regardless of the animal disease state, each NO-releasing implant tested elicited reduced inflammation compared to controls at both 3 and 10 d. However, only the NO-release materials capable of releasing low NO fluxes (0.8–3.3 pmol cm^{-2} s^{-1}) for 7–13 d durations mitigated the inflammatory response at 25 d. Using immunohistochemical staining for the endothelial cell surface marker CD-31, we also observed poor blood vessel development at non-NO-releasing implants in diabetic swine. Relative to controls, NO-releasing implants with the longest NO-release duration (13 d) increased blood vessel densities by 47.1 and 70.4% in the healthy and diabetic pigs, respectively. In the healthy model, tissues surrounding the long NO-release materials contained sparse amounts of collagen, whereas implants with shorter NO-release durations (2, 3, and 7 d) were characterized with a dense collagen encapsulation layer, similar to controls. Collagen deposition in diabetic swine was

[*]Corresponding author: schoenfisch@unc.edu Phone: (919) 843-8714, Fax: (919) 962-2388.

Author Contributions

This research was performed through contributions of all authors. RJS, EPM, DAB, TCN, and MHS were responsible for conceptualizing and planning the in vivo tissue response experiments. DAB was responsible for surgically implanting and explanting the test articles. EPM assisted with the surgeries, preserved, sectioned, and imaged the tissue slices, and provided expertise on pathological FBR evaluation. RJS fabricated the NO-releasing implants, analyzed the histological/immunohistochemical data, and wrote the manuscript. All authors were responsible for editing the manuscript and approve the final article.

Declaration of Interests

The corresponding author declares the following competing financial interest(s): Mark Schoenfisch maintains financial interest in Clinical Sensors, Inc and Novan, Inc. Clinical Sensors is developing NO-releasing sensor membranes for continuous glucose monitoring devices. Novan is commercializing NO-releasing macromolecular vehicles for dermatological indications.

inhibited, and unaffected by NO. These results emphasize several key differences in the FBR in the setting of acute onset diabetes. The observation that NO release counteracts the more severe FBR in diabetic swine while simultaneously promoting tissue integration may help guide the design of medical implants (e.g., glucose sensors) with improved performance for diabetes management.

Keywords

Diabetes; Foreign Body Response; Glucose Biosensor; Inflammatory Response; Nitric Oxide; Wound Healing

INTRODUCTION

In vivo glucose biosensors have been developed as technologies for continuous glucose monitoring of patients afflicted with diabetes mellitus [1]. Unfortunately, the in vivo analytical performance of such devices in subcutaneous tissue is compromised due to the foreign body response (FBR) [1–3]. Sensor insertion damages vascularized tissue, resulting in local bleeding and accumulation of proteins and protein fragments on the surface of the sensor [4]. The adsorbed protein layer is responsible for an immediate decrease (40–80%) in glucose sensitivity and serves as an anchor for cell adhesion [5]. Infiltration of the implant site by inflammatory cells (e.g., neutrophils, macrophages) [3] during the ensuing inflammatory response further impacts in vivo sensor performance [6–9]. For instance, pro-inflammatory macrophages have abnormally large metabolic demands and create glucose depletion zones in the sensor microenvironment [7,9]. Failure to digest the sensor incites frustrated phagocytosis and macrophage fusion to form foreign body giant cells [3]. Stress-cracking or delamination of sensor coatings by these polynuclear cells is a frequent cause of in vivo sensor failure [10]. Even for materials that are relatively insusceptible to oxidative damage (e.g., polycarbonate urethanes) [11], phagocytic activity by macrophages and giant cells may decrease the pH in the tissue surrounding the sensor (extreme pH values 3.6) [12] with the potential to interfere with the enzyme-based sensor response. Conclusion of the FBR is marked by the deposition of a dense, avascular collagen capsule around the implanted sensor. Capsule formation obstructs interstitial glucose transport and causes a pronounced temporal lag in the sensor signal, thereby preventing the sensor from accurately tracking glucose concentrations [8,13–14].

The analytical performance of in vivo glucose sensors is inherently linked with all aspects of the FBR [15]. Although the FBR has classically been studied as a function of material surface chemistry [16], proper selection of coating materials alone is insufficient to improve glucose sensor function. The most promising biocompatibility strategies have instead aimed to reduce inflammation and simultaneously guide wound healing at the sensor tissue interface. Topographical cues (i.e., porosity) [17], active release of anti-inflammatory agents (e.g., Dexamethasone) [18–19], and delivery of angiogenic stimulators (vascular endothelial growth factor, platelet-derived growth factor) [20] have all been investigated as approaches to reduce the FBR. Our laboratory has proposed the release of nitric oxide (NO) from polymeric implant coatings to mitigate the FBR [21–24]. Nitric oxide functions as an

angiogenic agent by upregulating vascular endothelial growth factor (VEGF) production [25–28]. NO also mediates inflammatory cell recruitment and phenotypes by regulating key cytokines/chemokines involved in the FBR (e.g., tumor necrosis factor-α, macrophage chemoattractant protein-1, interleukin-1β) [29–32], although the mechanisms for NO's involvement in inflammation have not been fully investigated.

Prior research in our laboratory has shown that NO-releasing surfaces reduce the FBR and improve attributes of glucose sensor performance [21–24,33]. Hetrick et al. first demonstrated the use of NO-releasing silica xerogels to mitigate FBR-related inflammation and collagen deposition in mouse subcutaneous tissue. Subsequent work by Nichols et al. revealed a dependence of the FBR on NO-release kinetics [22]. Subcutaneous implants capable of extended NO release (≥3 d) reduced inflammation and collagen deposition, whereas rapid release (≤24 h) lead to increased collagen encapsulation. Two separate studies have confirmed the benefits of NO release and a reduced FBR to in vivo glucose sensor accuracy [24,33].

Despite promising tissue histology and preclinical sensor performance data [21–24,33], each of these initial studies utilized healthy animal models. Relative to healthy tissue, diabetic wounds are generally characterized as having inadequate wound repair processes [34], altered inflammatory cell infiltration and cytokine production [35], and disrupted blood flow [36]. Reduced angiogenesis and cytokine production are features that are at least partially due to inhibited NO production [37–38]. These disparities have been characterized in the context of wound healing in humans, but the effects of a foreign body (i.e., an implanted glucose sensor) on inflammation and tissue reconstruction have not been studied in great detail. Furthermore, it is unclear if the benefits of NO, documented in previous tissue histology [21–22] and functional sensor experiments [24,33], will counteract the wound healing deficiencies concomitant with diabetes. Our hypothesis is that supplementing diabetic subcutaneous wounds with exogenous NO (i.e., from NO-releasing polymers) will help to offset the negative effects (i.e., altered angiogenesis and inflammation) arising from inhibited NO production.

Herein, the tissue responses to control and NO-releasing polyurethane materials are evaluated in both healthy and diabetic porcine models to generate new information on how diabetes impacts FBR-related inflammation and collagen deposition. Polymers capable of tunable NO release were employed to assess the role of NO on the FBR in diabetic tissue.

EXPERIMENTAL SECTION

Materials

Tetraethylorthosilicate (TEOS), *N*-(3-trimethoxypropyl)diethylenetriamine (DET) and 3-mercaptopropyltrimethoxysilane (MPTMS) were purchased from Gelest (Morrisville, PA) and stored under nitrogen. Aqueous ammonium hydroxide (NH_4OH; 29.41 wt% ammonia), sodium methoxide (NaOMe; 5.4 M in methanol), ethanol (EtOH; 200 proof), hydrochloric acid (HCl), all salts, and anhydrous solvents (*N,N*-dimethylformamide (DMF), tetrahydrofuran (THF), and methanol (MeOH)) were purchased from Fisher Scientific (Fair Lawn, NJ). Cetyltrimethylammonium bromide (CTAB) was purchased from Sigma (St

Louis, MO). Nitrogen (N_2), argon (Ar), and nitric oxide calibration (25.87 ppm in nitrogen) gases were purchased from Airgas National Welders (Raleigh, NC). Pure NO gas was purchased from Praxair (Danbury, CT). Soft stainless steel wire (356 μm dia.) was purchased from McMaster-Carr (Atlanta, GA). Tecoflex SG-85A (TPU) and Tecothane TT-2072D-B20 (TT) polyurethanes (PUs) were received from Lubrizol (Cleveland, OH). Streptozotocin was purchased as a sterile powder from Teva and reconstituted in sterile saline at 100 mg mL^{-1}. Water was purified to a resistivity of 18 M(cm and a total organic content of <6 ppb using a Millipore Reference water purification system.

Synthesis of NO donor-modified mesoporous silica nanoparticles

Mesoporous silica nanoparticles functionalized with either *N*-diazeniumdiolate or *S*-nitrosothiol (RSNO) NO donors were synthesized using variants of the Stöber method, as reported previously [39–40]. Detailed synthesis procedures are provided in the Supplementary Information section.

Preparation of nitric oxide-releasing polyurethane membrane-coated implants

Nitric oxide-releasing polymeric membranes were fabricated by doping control or NO donor-modified MSNs into biomedical-grade polyurethane (Tecothane TT-2072D-B20; TT). Polymer solutions were initially prepared by dissolving 360 mg polyurethane (PU) in THF (3.00 mL). The silica particles were dispersed in THF in a separate container, added to the PU solution, and vortexed. The final PU concentration was 80 mg mL^{-1} for all solutions. The final concentration of particles in the PU solution was 20 mg mL^{-1}. In cases of dual RSNO and DET/NO particle incorporation, two separate particle dispersions were prepared and added to the PU.

Stainless steel wire served as the substrate for depositing the NO-releasing PU composites due to similar geometry and size compared to needle-type glucose sensors (~350 μm diameter). The wire was initially cut into 7 cm pieces and sterilized in a steam autoclave. All subsequent coating procedures were carried out in a sterile biological safety cabinet. The wires were modified with the NO-releasing membranes via dipcoating into the PU/MSN solution and drying for 1 h. The total number of coats was 16. A TPU topcoat (60 mg mL^{-1} in THF) was applied to all membranes to minimize leaching of the MSNs from the membranes. The external PU coat also served to ensure consistent surface chemistry across the different implants, as surface chemistry could represent a convoluting variable with respect to FBR severity. The coated portion of the wire was cut to a final length of 15 mm prior to coating the exposed ends with the TPU topcoat solution. After drying (~1 h), the implants were housed individually in sterile microcentrifuge tubes and stored in a sterile vacuum-sealed Mylar bag at −80 °C until use. Control (i.e., non-NO-releasing) materials were prepared in an identical manner except that the particles were not functionalized to release NO. Of note, the control particles were washed 3× with sodium methoxide following the H^+ ion exchange step of the MSN purification process to remove ionically bound protons.

Membrane characterization

Nitric oxide release from the PU membranes was measured using a Sievers 280i chemiluminescence NO analyzer (NOA; Boulder, CO). The NOA was calibrated immediately before all measurements using air passed through an NO–zero filter as the blank value and 25.87 ppm NO (in nitrogen gas) as the second calibration standard. The NO-releasing membranes were immersed in phosphate buffered saline (PBS; 10 mM, pH 7.41) at 37 °C. For membranes that contained RSNO-modified particles, the NOA sample flask was shielded from light. In addition, 500 μM DTPA was added to the PBS to chelate trace copper ions, thus restricting NO release to thermal mechanisms. The NO released from the membranes was carried to the NOA by stream of nitrogen gas (80 mL min^{-1}) bubbled through the PBS solution. Supplemental nitrogen gas flow was provided to the NOA to match the 200 mL min^{-1} instrument intake. Nitric oxide was detected indirectly by chemiluminesce emission from excited-state nitrogen dioxide, formed by reaction between NO and ozone. Data was collected at a sampling frequency of 1 Hz, providing near real-time measurements of NO release from the PU membranes. Measurements were terminated when NO concentrations fell below the detection limit of the NOA (~6 ppb or 0.8 pmol cm^{-2} s^{-1}).

Particle leaching from the membranes was assessed by soaking membranes in PBS for a pre-determined period of time (1–28 d) and measuring the silicon content of soak solutions via inductively coupled plasma optical emission spectrometry (ICP-OES; Teledyne-Leeman Labs Prodigy high-dispersion ICP; Hudson, NH). The instrument was initially calibrated using sodium silicate standards in PBS (0.1–25 ppm; 251.611 nm Si emission line) to ensure linear response over the anticipated range of particle concentrations. Calibration curves were subsequently generated for each type of silica particle and compared to Si emission intensity values from the membrane soak solutions for leaching determination.

In vivo protocol

All procedures and protocols were in accordance with institutional guidelines and approved by the Institutional Animal Care and Use Committee at the University of North Carolina in Chapel Hill. Twelve mixed gender Yorkshire-type piglets, weighing approximately 12–17 kg at the study onset, were used. Diabetes was induced in half of the piglets (three males and three females) by repeated intravascular administration of streptozotocin (25–50 mg kg^{-1}, 3–4 doses over 4–6 d) until elevated post-prandial blood glucose values (171 ± 50 mg dL^{-1}, mean ± standard deviation) were consistently observed in ear prick glucose measurements. Pooled blood glucose values for controls (i.e., without STZ treatment) were 61 ± 18 mg dL^{-1}. The pigs were maintained for 2–6 days prior to implanting the mock sensors. On the day of implantation, the pigs were initially sedated with Telazol. Anesthesia was maintained with isoflurane delivered through an endotracheal tube. The mock sensors were implanted using aseptic technique by cannulation into the subcutaneous tissue using a 18 G catheter inserter. The implants were organized into 4 groups on either side of the spine to control for variability due to implant location, for a total of two implants of each type per animal (4 implants per time point and disease state). After a pre-determined period of time (3, 10, or 25 d), the pigs were euthanized and the test articles located using a portable X-ray imaging system. Tissues surrounding the mock sensors were explanted en bloc and fixed in 10 vol% buffered formalin. Thin, serial sections (~5 μm) were stained with hematoxylin and eosin

(H&E) or Masson's Trichrome for visualization of inflammatory cells or collagen, respectively. Following an antigen retrieval step, immunohistochemical analysis for cluster of differentiation marker 31 (CD31), an endothelial cell surface marker, was carried out using pig-reactive anti-CD31 antibodies from Abcam (ab28364; 1:500 dilution of stock antibody).

The severity of the inflammatory response was assessed from photomicrographs of hematoxylin and eosin-stained tissue slices. The number of inflammatory cells (e.g., neutrophils, macrophages) within ~200 μm of the implant surface was counted by a blinded observer. Average numbers of inflammatory cells (ICs), normalized to the tissue area (i.e., IC densities), served as indicators of inflammatory response severity. Of note, these counts excluded extravasated erythrocytes, which are not associated with the FBR. Collagen deposition was quantified within 200 μm of the implant surface similarly to previous reports [21–22,41] using Masson's Trichrome-stained tissue sections. Portions of the photomicrographs that stained blue, originating from collagen fibers, were isolated using a color filter in photoshop and then inverted so that white pixels corresponded to collagen fibers. Regions 200×50 μm in size were then cropped from the image and saved as text images. A custom MATLAB script was used to determine a percent collagen density by comparing the number of white pixels to the total number of pixels in the image. Immunohistochemical staining for CD31 was employed to quantitatively evaluate angiogenesis by counting the total number of blood vessels, identified as open tubular brown structures, within 400 μm of the implant surface.

Statistical analysis

Inflammatory cell densities and collagen deposition data were tested for normality using a Shapiro-Wilk test. In all cases, the data were determined to be distributed normally at >99% confidence. Thus, the data were analyzed using a two-tailed student's t-test with p-values <0.05 considered statistically significant. For multiple comparisons, one-way Analysis of Variance was used followed by individual comparisons using a student's t-test with an applied Bonferroni correction.

RESULTS AND DISCUSSION

Polyurethane materials with diverse NO-release properties were fabricated by doping Tecothane (TT) PU membranes with two different types of NO-releasing MSNs (Figure 1). The NO-releasing polymers were coated onto steel wire substrates that mimicked the size and geometry of needle-type electrochemical glucose biosensors used in previous studies [24,33]. The mock sensors were further modified with a TPU topcoat that normalized the surface chemistry of all implants. The membrane NO-release kinetics were intentionally manipulated by careful selection of the NO donor modification on the silica particle dopants. For instance, the *N*-diazeniumdiolate moiety (i.e., the DET particle NO donor modification) undergoes proton-initiated decomposition to release NO at rates dependent on pH, temperature, and the chemical structure of the precursor amine [42]. By incorporating the NO donor-modified DET particles into a hydrophobic aromatic Tecothane PU, proton access to the *N*-diazeniumdiolate moiety is reduced, thus prolonging NO release. The resulting

membranes (DET/NO) released low NO fluxes (1–12 pmol cm^{-2} s^{-1}) for ~13 d (Table 1). To achieve more rapid NO release, MSNs modified with *S*-nitrosothiol NO donors (RSNOs) were co-incorporated with DET/NO particles in Tecothane PU. *S*-nitrosothiols undergo thermally initiated S–N bond cleavage in vivo and thus have NO-release kinetics largely independent of the water uptake of the surrounding polymer matrix. Membranes prepared exclusively with RSNO particles released large, maximum NO fluxes (630 pmol cm^{-2} s^{-1}) and exhausted their NO supply within 48 h (Table 1; Figure 2). Materials incorporating both types of NO donor-modified MSNs (at 3:1 and 1:1 RSNO:DET mass ratios) released more intermediate NO fluxes initially (285 and 200 pmol cm^{-2} s^{-1}, respectively) and maintained NO release above >0.8 pmol cm^{-2} s^{-1} for longer durations (3 and 7 d, respectively) than the RSNO system alone. The four NO-releasing membranes that were chosen for evaluation (i.e., DET/NO, 3:1 RSNO:DET, 1:1 RSNO:DET, and RSNO) release sufficient amounts of NO (>1.5 μmol cm^{-2}, Figure S1) at fluxes shown to mitigate the FBR in healthy animal models (1–384 pmol cm^{-2} s^{-1}) [21–22]. The membranes also release NO for durations that align with the anticipated timelines of the acute and chronic inflammatory responses (~1–2 and 3–14 d, respectively) [3,43–44].

Although silica is generally tolerable in vivo [45], leaching of the NO-releasing particles from the PU membranes could prove problematic, as silica nanoparticles may be phagocytosed by macrophages, increasing production of pro-inflammatory cytokines (e.g., interleukin-1β, tumor necrosis factor-α) [46–47]. Given the potential for leachable silica to offset any favorable effects of NO on the FBR, we assessed particle leaching from the MSN-doped membranes. Quantitative ICP-OES analysis of silicon concentrations in membrane soak solutions indicated minimal (<5%) silica particle leaching from each of the NO-releasing and control membranes. The materials were thus deemed suitable for further evaluation of the FBR.

Inflammatory response

A porcine model was selected for FBR evaluation due to similarities in subcutaneous tissue composition (i.e., proportion of adipose tissue and collagen content) between pigs and humans [48–51]. Chemical induction of diabetes was carried out by administrating multiple doses of the pancreatic β-cell cytotoxin, streptozotocin (STZ), over a 4–6 d period preceding implantation of the materials. Diabetes induction in the pigs was confirmed by greater post-prandial blood glucose values relative to untreated pigs (171 ± 50 and 61 ± 18 mg dL^{-1}, respectively; Figure S2). Hyperglycemia was maintained for the entire study duration (i.e., 1 mo) using this protocol.

Inflammatory cells negatively impact glucose sensor performance, due in part to their large, localized glucose/oxygen consumption and ability to damage sensor components via respiratory bursts (i.e., release of reactive oxygen and nitrogen species) [7–8,10,12]. Elevated inflammatory cell presence is consistently linked to poor sensor performance [7–9]. As such, photomicrographs of hematoxylin and eosin-stained tissues were used to quantitatively assess the inflammatory response. The severity of the inflammatory response was determined at three different implantation periods (3, 10, and 25 d) and considered with respect to both NO and animal model disease state. The 3 d tissue response consisted

primarily of macrophages (based on nuclear morphologies observed in the hematoxylin and eosin stains; Figure 3), indicating the 3 d time point corresponded to onset of the chronic inflammatory response [3]. This inflammatory response was largely localized to ~100 μm from the implant surface, while unperturbed tissues (>10 mm from control implants) were only sparsely populated with cells (Figure S4). Inflammatory cell densities adjacent to control (non-NO-releasing) implants at 3 d were similar between the healthy and diabetic pigs (~3.3–3.9×10^3 cells mm^{-2}), indicating that diabetes does not impact initial cell recruitment. Release of NO during the first 3 d elicited a modest reduction in the inflammatory response for the healthy pigs (10–30%; Figure 4A), although these differences were largely statistically insignificant. Inflammation was mitigated to a greater degree by NO in the STZ-treated pigs, with 35–50% reductions in the number of ICs at NO-releasing implants relative to controls (Figure 4B). There were no significant differences between the NO-releasing membranes in the healthy or diabetic pigs (ANOVA p-values 0.46 and 0.62, respectively), indicating the large initial NO fluxes (18–630 pmol cm^{-2} s^{-1}) released by the RSNO-based membranes over the first 4 h, did not impact cell presence to a greater extent than the DET/NO system (NO concentrations <12 pmol cm^{-2} s^{-1}). Lower NO fluxes, released gradually during the first 2–3 d in which FBR-associated cells infiltrate the implant site, thus appear to be responsible for the reduced inflammatory response.

A more severe inflammatory response was observed for control implants after 10 d relative to the initial (3 d) time point (Figures 3F and 3H). For example, IC counts for the RSNO controls in the healthy and diabetic animals were 6.0×10^3 and 6.2×10^3 cells mm^{-2}, respectively, compared to 3–4×10^3 cells mm^{-2} at 3 d. A reduced inflammatory response was evident at most NO-releasing implants in both animal models (Figures 4C and 4D). In healthy swine, low, sustained NO release from the DET/NO membranes (i.e., 1–12 pmol cm^{-2} s^{-1} for 13 d) resulted in fewer inflammatory cells than the more rapid RSNO or 3:1 RSNO:DET NO-release systems. In agreement with previous work [22], this result suggests that materials with more extended NO-release kinetics more favorably mitigate the inflammatory response. However, there were no discernable differences arising from varying NO-release kinetics in the diabetic pig model (ANOVA p=0.364).

Additional cell recruitment to the implant site ceased after 10 d in the healthy swine model, indicating resolution of the initial inflammatory response. Indeed, IC counts at 10 and 25 d post-implantation were similar for both sets of controls. In contrast, the inflammatory response became more severe in the diabetic pigs. Inflammatory cell densities nearly doubled after 25 d in comparison to the 10 d values for DET controls (12.4×10^3 and 6.4×10^3 cells mm^{-2}, respectively; p=0.006), and the inflammatory response for RSNO controls was similarly elevated (8.5×10^3 and 6.2×10^3 cells mm^{-2}; p=0.031). In a previous investigation, Wang et al. also observed a delayed inflammatory response in STZ-induced diabetic rats, although the number of cells decreased between 10 and 25 d [52]. The use of a porcine model in our study may account for the disagreement. This difference notwithstanding, the persistent inflammation observed in the diabetic pigs was not surprising, as a delayed inflammatory response is a known outcome of diabetes [38].

Although the 2–3 d NO-release systems (i.e., RSNO and 3:1 RSNO:DET) were characterized with low degrees of inflammation at 3 and 10 d, the inflammatory responses to

these membranes became similar to controls at 25 d post-implantation. In agreement with a previous study [22], short-term NO release proved incapable of lessening the chronic FBR in healthy pigs (Figure 4E). The degree of inflammation in the diabetic pigs was also comparable between controls and the 2–3 d NO-releasing membranes. In contrast, the more extended NO-release systems (i.e., DET/NO and 1:1 RSNO:DET) maintained low IC densities ($2–5\times10^3$ cells mm^{-2}), a state akin to the quiescent inflammatory responses observed at 3 d. Although this data highlights a unique benefit of extended NO release, it is unclear as to how 7–13 d of active NO release impacts inflammation up to 18 d later. This feature was also evident for the 2–3 d NO-release systems, which reduced the inflammatory response at 10 d. These observations are consistent with prior work by Hetrick et al. [21] and Nichols et al. [22]. Although these effects are not fully understood, NO is a known mediator of several key chemokines/cytokines involved in cell recruitment during the FBR, including tumor necrosis factor-α, macrophage chemoattractant-1, and interleukin-1β [29–32]. In this regard, NO may delay inflammatory cell recruitment to the implant site, thus resulting in prolonged effects even when NO is not actively generated.

Collagen deposition

The most often observed outcome in the FBR to indwelling glucose biosensors is the formation of a dense, collagenous tissue layer segregating the sensor from the surrounding extracellular matrix [8,13–14]. This collagen layer lacks the extensive vascular network of subcutaneous tissue and is populated by metabolically active inflammatory cells, which consume glucose in the immediate vicinity. Compounding the issue of glucose availability, the collagen capsule is characteristically dense and is an effective transport barrier to interstitial glucose that could otherwise be detected by the glucose sensor. As a consequence, collagen encapsulation causes attenuation of the glucose sensor signal and a pronounced temporal lag (20–30 min relative to blood), ultimately resulting in sensor failure [8]. Nitric oxide, released from a surface, can reduce collagen deposition at subcutaneous implants in healthy animals [21–22], likely due to NO's involvement in the production of transforming growth factor β (TGF-x) [26] a stimulator of collagen production by fibroblasts [53]. However, the impaired wound healing associated with diabetes is at least partly the result of disrupted collagen deposition [34,38] which may alter the degree to which an implant is encapsulated during the FBR and/or potential benefits of NO. As such, collagen in the regions surrounding the mock sensors was visualized in tissue slices stained with Masson's Trichrome. Photomicrographs of the stained tissues were then used to quantify collagen deposition proximal to the implant surface (within 200 μm) as a percentage (density) of the total image area occupied by blue collagen pixels.

Stained samples immediately adjacent to the implants are shown in Figure 5, and micrographs of tissues >10 mm away from the implant are provided for comparison in the Supplementary Information section (Figure S4). Of note, collagen analysis was not carried out at 3 d as the collagen was sparse with no apparent capsule formation around the implants (Figures A–D). By 10 d, a dense capsular layer (collagen densities ~20–30%) had formed around most of the control and NO-releasing implants in the healthy pigs (Figures 5E–H and 6A). After 25 d, typical collagen densities had increased to ~30–50% (Figures 5E–L and 6B). The progressive isolation of control materials by the collagen capsule during the first

several weeks implantation was expected [3,13–14,21–22,54]. Similar to controls, a significant amount of collagen surrounded the NO-releasing membranes with the exception of the longest NO-release system (DET/NO), with <14% collagen density at both 10 and 25 d.

Relative to observations in the healthy pigs, collagen deposition was markedly lower in tissue samples harvested from the diabetic swine. Typical % collagen values were in the range of 5.8–11.5% after 10 d for all samples in the STZ-treated model compared to 9.2–29.8% in the healthy pigs. Even more disparate collagen density values were observed at 25 d (11.8–17.4% vs. 29.7–50.0% for the diabetic and control pigs, respectively). No discernable difference was noted in the % collagen values between any of the implants (control or NO-releasing) in the diabetic pigs at either 10 or 25 d (ANOVA p-values 0.80 and 0.87, respectively). In agreement with our results, at least two investigations have shown that collagen deposition is inhibited during the FBR in diabetic animals [55–56]. In one of these studies, the authors suggested that reduced collagen deposition was due to low levels of TGF-β in diabetic rats [55]. As NO suppresses TGF-β levels [26], low levels of endogenous TGF-β may account for both the low amounts of collagen at control implants and the lack of an observable effect at the NO-releasing membranes.

Angiogenesis

Glucose sensor implantation disrupts native tissue and destroys vascular structures in the immediate vicinity of the device. As the sensor becomes progressively more isolated by inflammatory cells and collagen during the FBR, the proximal tissue remains void of vasculature. The lack of blood vessels at the implant site prevents consistent glucose transport to the sensor, reducing glucose concentrations at the implant surface and thereby contributing to erratic sensor response [8,14,54,57]. Adequate vascularization has thus been suggested as a key requirement for ensuring consistent glucose sensor function [8,14,54]. Unfortunately, evidence that diabetes impairs angiogenesis [34,37–38] suggests an even more unfavorable sensor environment with respect to vascular glucose transport. In this respect, NO's well-known angiogenic capabilities [25–28] may improve blood vessel density in the implant microenvironment.

We selected DET/NO and analogous control membranes for further evaluation of blood vessel formation (10 d) because this NO-releasing formulation most effectively mitigated inflammation and collagen deposition. Vessels in the vicinity of the implants were visualized by immunohistochemical staining for the endothelial cell surface marker CD31. Representative photomicrographs of the tissue samples (counterstained with hematoxylin), both adjacent to the implants and >10 mm away, are provided in Figure 7 and Figure S5, respectively. Blood vessel counts, presented graphically in Figure 8, were compared between the healthy and diabetic pigs for DET controls (63 and 47 vessels per field, respectively), revealing a potential difference that approached statistical significance (p=0.095). This observation is consistent with one other study, demonstrating reduced angiogenesis in STZ-induced diabetic rats [55]. In contrast to the controls, tissues surrounding the NO-releasing implants were significantly more vascularized in both the healthy (93 vessels per field) and diabetic (81 vessels per field) models. This result was somewhat expected, as NO derived

from endothelial nitric oxide synthase is an essential component of angiogenesis during tissue remodeling [28]. Several pro-angiogenic growth factors (e.g., VEGF) elicit NO production [26,58]. In addition, NO has been shown to stimulate VEGF expression [25]. Hetrick et al. also reported increased blood vessel formation in healthy rats using materials capable of releasing 1–110 pmol NO cm^{-2} s^{-1} [21]. Our work expands on this previous investigation, demonstrating that lower fluxes of exogenous NO (~1–12 pmol cm^{-2} s^{-1}) are proangiogenic in both healthy and diabetic swine.

CONCLUSIONS

Prior research has established the utility of polymeric NO release for reducing FBR-related inflammation and collagen deposition [21–23] and, in turn, positively influencing the analytical performance of in vivo glucose biosensors [24,33]. However, insufficient literature regarding the impact of diabetes on the FBR brings into question the relevance of this data. The research presented herein represents an important step to understanding differences in the FBR in the context of acutely-induced diabetes. In particular, a delayed—but more severe—inflammatory response was a unique feature in diabetic pigs. Nitric oxide release from the polyurethane materials mitigated the early inflammatory response (i.e., at 3 and 10 d) in both models, highlighting a key anti-inflammatory benefit associated with this strategy. However, only long-term NO-releasing implants maintained low degrees of inflammation at extended periods (25 d), counteracting the severe chronic inflammation in the diabetic swine. Sustained NO release also stimulated angiogenesis at the implant-tissue interface in both the healthy and diabetic swine models. Collectively, we confirm that the anti-inflammatory and pro-angiogenic properties of NO are preserved regardless of disease state. However, a key distinction associated with the FBR in the diabetic swine model was the comparatively low degree of capsular tissue formation. Although long-term NO release was effective at reducing collagen in healthy pigs, the already minimal amounts of collagen in the diabetic pigs appeared to be unaffected by NO, regardless of NO-release kinetics. This apparent inhibition of collagen deposition in the diabetic pigs serves to caution against extrapolating histological outcomes in healthy animal models to anticipated results in diabetic tissue.

There are several aspects of this work that warrant a more detailed study of the FBR. Although the developed NO-releasing membranes have overt effects on the FBR in both animal models, the biological processes underlying these differences are not well understood. Indeed, the mechanisms proposed in this publication are merely speculative, based on past literature rather than direct experimental evidence from this work. Analysis of key FBR cytokines (transforming growth factor β, interleukin, 1β, tumor necrosis factor α, etc.), macrophage polarization markers (cluster of differentiation 163, major histocompatibility complex class II, etc.), and cell populations may shed light on more subtle aspects of NO’s influence. A similar approach could also be used to examine effects of silica particle leaching; although efforts were taken to minimize particle leaching in this work, we cannot entirely eliminate leaching as a convoluting variable. Planning and execution of these experiments are ongoing.

Supplementary Material

Refer to Web version on PubMed Central for supplementary material.

ACKNOWLEDGEMENTS

This research was supported by the National Institutes of Health (NIH DK108318–01) and the National Science Foundation (DMR 1104892). RJS gratefully acknowledges a John Motley Morehead dissertation fellowship from the Royster Society of Fellows at the University of North Carolina at Chapel Hill.

REFERENCES

[1]. Nichols SP; Koh A; Storm WL; Shin JH; Schoenfisch MH Biocompatible materials for continuous glucose monitoring devices. Chem Rev 2013, 113, 2528–2549. [PubMed: 23387395]

[2]. Cunningham DD; Stenken JA In vivo glucose sensing. Wiley: 2009.

[3]. Anderson JM; Rodriguez A; Chang DT Foreign body reaction to biomaterials. Sem Immunol 2008, 20, 86–100.

[4]. Gifford R; Kehoe JJ; Barnes SL; Kornilayev BA; Alterman MA; Wilson GS Protein interactions with subcutaneously implanted biosensors. Biomaterials 2006, 27, 2587–2598. [PubMed: 16364432]

[5]. Thévenot DR; Toth K; Durst RA; Wilson GS Electrochemical biosensors: Recommended definitions and classification. Biosens Bioelectron 2001, 16, 121–131. [PubMed: 11261847]

[6]. Avula MN; Rao AN; McGill LD; Grainger DW; Solzbacher F Foreign body response to subcutaneous biomaterial implants in a mast cell-deficient KIT(W-SH) murine model. Acta Biomater 2014, 10, 1856–1863. [PubMed: 24406200]

[7]. Klueh U; Qiao Y; Frailey JT; Kreutzer DL Impact of macrophage deficiency and depletion on continuous glucose monitoring in vivo. Biomaterials 2014, 35, 1789–1796. [PubMed: 24331705]

[8]. Novak MT; Yuan F; Reichert WM Modeling the relative impact of capsular tissue effects on implanted glucose sensor time lag and signal attenuation. Anal Bioanal Chem 2010, 398, 1695–1705. [PubMed: 20803006]

[9]. Novak MT; Yuan F; Reichert WM Macrophage embedded fibrin gels: An in vitro platform for assessing inflammation effects on implantable glucose sensors. Biomaterials 2014, 35, 9563–9572. [PubMed: 25175597]

[10]. Zhao Q; Topham N; Anderson JM; Hiltner A; Lodoen G; Payet CR Foreign-body giant cells and polyurethane biostability: In vivo correlation of cell adhesion and surface cracking. J Biomed Mater Res 1991, 25, 177–183. [PubMed: 2055915]

[11]. Christenson EM; Anderson JM; Hiltner A Oxidative mechanisms of poly(carbonate urethane) and poly(ether urethane) biodegradation: In vivo and in vitro correlations. J Biomed Mater Res A 2004, 70A, 245–255.

[12]. Wilson GS; Johnson MA In-vivo electrochemistry: What can we learn about living systems? Chem Rev 2008, 108, 2462–2481. [PubMed: 18558752]

[13]. Sharkawy AA; Klitzman B; Truskey GA; Reichert WM Engineering the tissue which encapsulates subcutaneous implants. I. Diffusion properties. J Biomed Mater Res 1997, 37, 401–412. [PubMed: 9368145]

[14]. Sharkawy AA; Klitzman B; Truskey GA; Reichert WM Engineering the tissue which encapsulates subcutaneous implants. II. Plasma-tissue exchange properties. J Biomed Mater Res 1998, 40, 586–597. [PubMed: 9599035]

[15]. Williams DF On the mechanisms of biocompatibility. Biomaterials 2008, 29, 2941–2953. [PubMed: 18440630]

[16]. Brodbeck WG; Shive MS; Colton E; Nakayama Y; Matsuda T; Anderson JM Influence of biomaterial surface chemistry on the apoptosis of adherent cells. J Biomed Mater Res 2001, 55, 661–668. [PubMed: 11288096]

[17]. Brown BN; Ratner BD; Goodman SB; Amar S; Badylak SF Macrophage polarization: An opportunity for improved outcomes in biomaterials and regenerative medicine. Biomaterials 2012, 33, 3792–3802. [PubMed: 22386919]

[18]. Vallejo-Heligon SG; Brown NL; Reichert WM; Klitzman B Porous, dexamethasone-loaded polyurethane coatings extend performance window of implantable glucose sensors in vivo. Acta Biomater 2016, 30, 106–115. [PubMed: 26537203]

[19]. Vallejo-Heligon SG; Klitzman B; Reichert WM Characterization of porous, dexamethasone-releasing polyurethane coatings for glucose sensors. Acta Biomater 2014, 10, 4629–4638. [PubMed: 25065548]

[20]. Kastellorizios M; Papadimitrakopoulos F; Burgess DJ Multiple tissue response modifiers to promote angiogenesis and prevent the foreign body reaction around subcutaneous implants. J Control Release 2015, 214, 103–111. [PubMed: 26216396]

[21]. Hetrick EM; Prichard HL; Klitzman B; Schoenfisch MH Reduced foreign body response at nitric oxide-releasing subcutaneous implants. Biomaterials 2007, 28, 4571–4580. [PubMed: 17681598]

[22]. Nichols SP; Koh A; Brown NL; Rose MB; Sun B; Slomberg DL; Riccio DA; Klitzman B; Schoenfisch MH The effect of nitric oxide surface flux on the foreign body response to subcutaneous implants. Biomaterials 2012, 33, 6305–6312. [PubMed: 22748919]

[23]. Nichols SP; Le NN; Klitzman B; Schoenfisch MH Increased in vivo glucose recovery via nitric oxide release. Anal Chem 2011, 83, 1180–1184. [PubMed: 21235247]

[24]. Soto RJ; Privett BJ; Schoenfisch MH In vivo analytical performance of nitric oxide-releasing glucose biosensors. Anal Chem 2014, 86, 7141–7149. [PubMed: 24984031]

[25]. Dulak J; Jozkowicz A; Dembinska-Kiec A; Guevara I; Zdzienicka A; Zmudzinska-Grochot D; Florek I; Wojtowicz A; Szuba A; Cooke JP Nitric oxide induces the synthesis of vascular endothelial growth factor by rat vascular smooth muscle cells. Arterioscler Thromb Vasc Biol 2000, 20, 659–666. [PubMed: 10712388]

[26]. Inoue N; Venema RC; Sayegh HS; Ohara Y; Murphy TJ; Harrison DG Molecular regulation of the bovine endothelial cell nitric oxide synthase by transforming growth factor-beta 1. Arterioscler Thromb Vasc Biol 1995, 15, 1255–1261. [PubMed: 7543000]

[27]. Cooke JP NO and angiogenesis. Atheroscler Suppl 2003, 4, 53–60. [PubMed: 14664903]

[28]. Cooke JP; Losordo DW Nitric oxide and angiogenesis. Circulation 2002, 105, 2133–2135. [PubMed: 11994243]

[29]. Deakin AM; Payne AN; Whittle BJ; Moncada S The modulation of IL-6 and TNF-alpha release by nitric oxide following stimulation of j774 cells with LPS and IFN-gamma. Cytokine 1995, 7, 408–416. [PubMed: 7578978]

[30]. Wetzler C; Kampfer H; Pfeilschifter J; Frank S Keratinocyte-derived chemotactic cytokines: Expressional modulation by nitric oxide in vitro and during cutaneous wound repair in vivo. Biochem Biophys Res Commun 2000, 274, 689–696. [PubMed: 10924337]

[31]. Bogdan C Nitric oxide and the immune response. Nat Immunol 2001, 2, 907–916. [PubMed: 11577346]

[32]. MacMicking J; Xie QW; Nathan C Nitric oxide and macrophage function. Annu Rev Immunol 1997, 15, 323–350. [PubMed: 9143691]

[33]. Gifford R; Batchelor MM; Lee Y; Gokulrangan G; Meyerhoff ME; Wilson GS Mediation of in vivo glucose sensor inflammatory response via nitric oxide release. J Biomed Mater Res A 2005, 75, 755–766. [PubMed: 16138325]

[34]. Schaper NC; Apelqvist J; Bakker K Reducing lower leg amputations in diabetes: A challenge for patients, healthcare providers and the healthcare system. Diabetologia 2012, 55, 1869–1872. [PubMed: 22622617]

[35]. Fahey TJ; Sadaty A; Jones WG; Barber A; Smoller B; Shires GT Diabetes impairs the late inflammatory response to wound healing. J Surg Res 1991, 50, 308–313. [PubMed: 2020184]

[36]. Vinik AI; Maser RE; Mitchell BD; Freeman R Diabetic autonomic neuropathy. Diabetes Care 2003, 26, 1553–1579. [PubMed: 12716821]

[37]. Witte MB; Kiyama T; Barbul A Nitric oxide enhances experimental wound healing in diabetes. Br J Surg 2002, 89, 1594–1601. [PubMed: 12445072]

[38]. Le NN; Rose MB; Levinson H; Klitzman B Implant healing in experimental animal models of diabetes. J Diabetes Sci Technol 2011, 5, 605–618. [PubMed: 21722576]

[39]. Riccio DA; Nugent JL; Schoenfisch MH Stöber synthesis of nitric oxide-releasing *S*-nitrosothiol-modified silica particles. Chem Mater 2011, 23, 1727–1735. [PubMed: 21499510]

[40]. Soto RJ; Yang L; Schoenfisch MH Functionalized mesoporous silica via an aminosilane surfactant ion exchange reaction: Controlled scaffold design and nitric oxide release. ACS Appl Mater Interfaces 2016, 8, 2220–2231. [PubMed: 26717238]

[41]. Koschwanez HE; Yap FY; Klitzman B; Reichert WM In vitro and in vivo characterization of porous poly-l-lactic acid coatings for subcutaneously implanted glucose sensors. J Biomed Mater Res A 2008, 87, 792–807. [PubMed: 18200540]

[42]. Keefer LK Fifty years of diazeniumdiolate research. From laboratory curiosity to broad-spectrum biomedical advances. ACS Chem Biol 2011, 6, 1147–1155. [PubMed: 21932836]

[43]. Wilson GS; Ammam M In vivo biosensors. FEBS Journal 2007, 274, 5452–5461. [PubMed: 17937773]

[44]. Wilson GS; Gifford R Biosensors for real-time in vivo measurements. Biosens Bioelectron 2005, 20, 2388–2403. [PubMed: 15854814]

[45]. Chen G; Roy I; Yang C; Prasad PN Nanochemistry and nanomedicine for nanoparticle-based diagnostics and therapy. Chem Rev 2016, 116, 2826–2885. [PubMed: 26799741]

[46]. Kusaka T; Nakayama M; Nakamura K; Ishimiya M; Furusawa E; Ogasawara K Effect of silica particle size on macrophage inflammatory responses. PLoS ONE 2014, 9, e92634. [PubMed: 24681489]

[47]. Waters KM; Masiello LM; Zangar RC; Tarasevich BJ; Karin NJ; Quesenberry RD; Bandyopadhyay S; Teeguarden JG; Pounds JG; Thrall BD Macrophage responses to silica nanoparticles are highly conserved across particle sizes. Toxicol Sci 2009, 107, 553–569. [PubMed: 19073995]

[48]. Koschwanez HE; Reichert WM In vitro, in vivo and post explantation testing of glucose-detecting biosensors: Current methods and recommendations. Biomaterials 2007, 28, 3687–3703. [PubMed: 17524479]

[49]. Larsen MO; Rolin B Use of the göttingen minipig as a model of diabetes, with special focus on type 1 diabetes research. ILAR J 2004, 45, 303–313. [PubMed: 15229377]

[50]. Swindle MM; Makin A; Herron AJ; Clubb FJ; Frazier KS Swine as models in biomedical research and toxicology testing. Vet Pathol 2012, 49, 344–356. [PubMed: 21441112]

[51]. Bellinger DA; Merricks EP; Nichols TC Swine models of type 2 diabetes mellitus: Insulin resistance, glucose tolerance, and cardiovascular complications. ILAR J 2006, 47, 243–258. [PubMed: 16804199]

[52]. Wang Y; Papadimitrakopoulos F; Burgess DJ Polymeric “smart” coatings to prevent foreign body response to implantable biosensors. J Control Release 2013, 169, 341–347. [PubMed: 23298616]

[53]. Chu AJ; Prasad JK Up-regulation by human recombinant transforming growth factor beta-1 of collagen production in cultured dermal fibroblasts is mediated by the inhibition of nitric oxide signaling. J Am Coll Surg 1999, 188, 271–280. [PubMed: 10065816]

[54]. Sharkawy AA; Klitzman B; Truskey GA; Reichert WM Engineering the tissue which encapsulates subcutaneous implants. III. Effective tissue response times. J Biomed Mater Res 1998, 40, 598–605. [PubMed: 9599036]

[55]. Socarras TO; Vasconcelos AC; Campos PP; Pereira NB; Souza JP; Andrade SP Foreign body response to subcutaneous implants in diabetic rats. PLoS One 2014, 9, e110945. [PubMed: 25372281]

[56]. Thomson SE; McLennan SV; Hennessy A; Boughton P; Bonner J; Zoellner H; Yue DK; Twigg SM A novel primate model of delayed wound healing in diabetes: Dysregulation of connective tissue growth factor. Diabetologia 2010, 53, 572–583. [PubMed: 20091023]

[57]. Paul DW; Stenken JA A review of flux considerations for in vivo neurochemical measurements. Analyst 2015, 140, 3709–3730. [PubMed: 25977941]

[58]. van der Zee R; Murohara T; Luo Z; Zollmann F; Passeri J; Lekutat C; Isner JM Vascular endothelial growth factor/vascular permeability factor augments nitric oxide release from

quiescent rabbit and human vascular endothelium. Circulation 1997, 95, 1030–1037. [PubMed: 9054767]

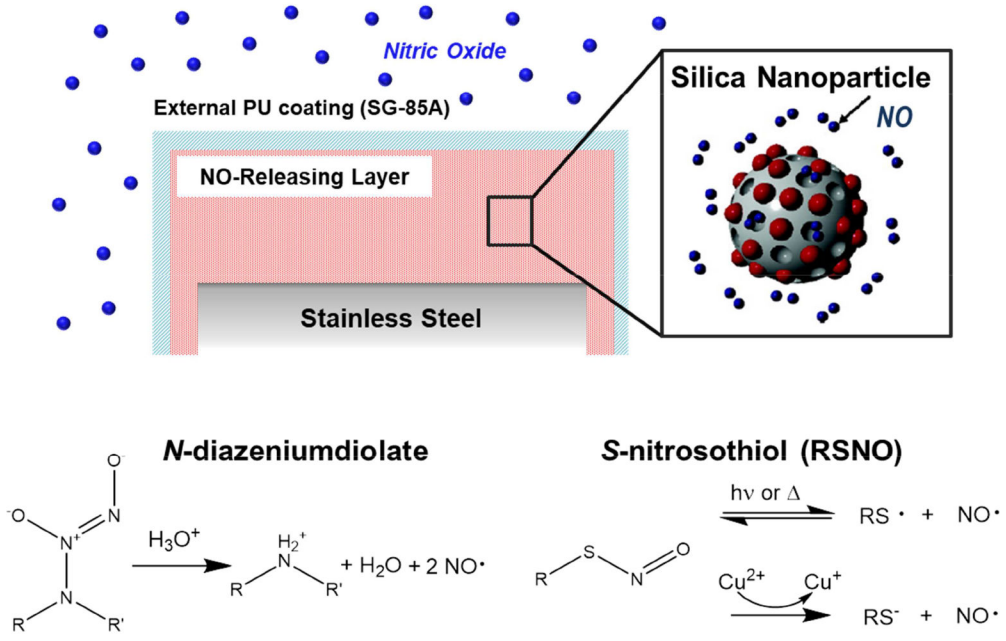

Figure 1.

Schematic of NO-releasing subcutaneous implants. The NO-releasing silica nanoparticles were doped into TT polyurethane membranes. An external TPU coating was applied to limit particle leaching and ensure consistent surface chemistry for all implant types. The implants released NO upon decomposition of the NO donors in vivo by either reaction with protons (*N*-diazeniumdiolates) or through a thermal mechanism (*S*-nitrosothiols).

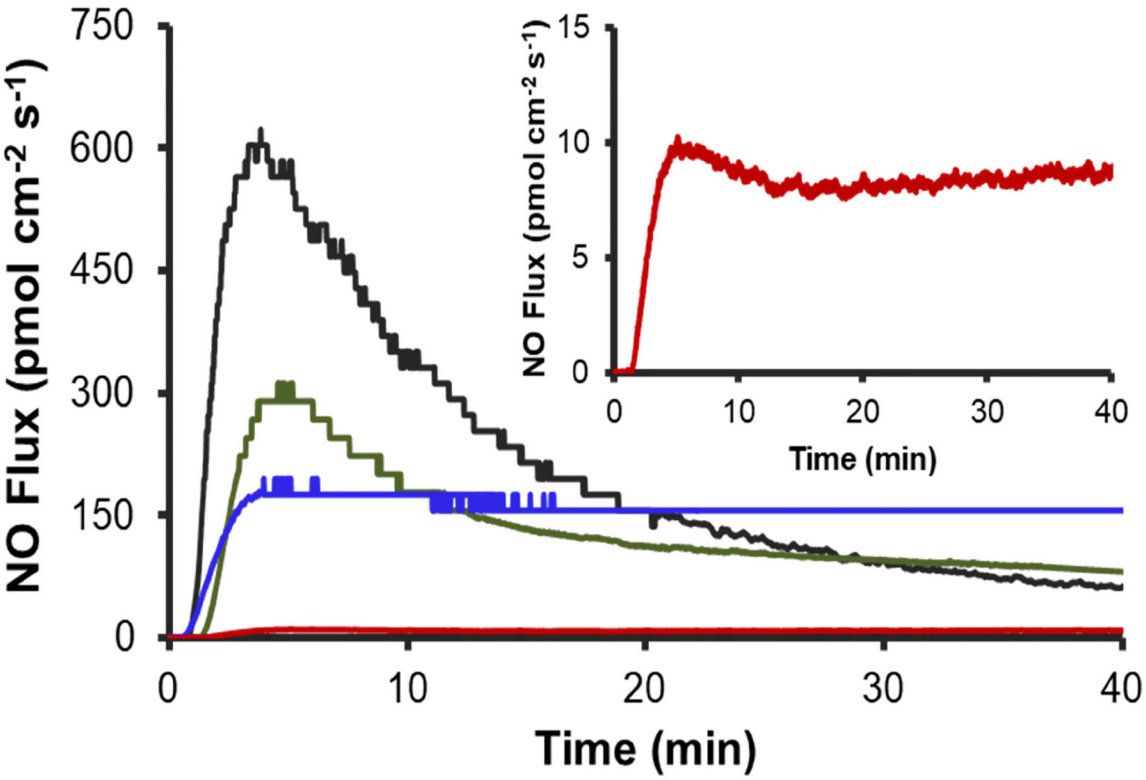

Figure 2.

Initial (40 min) NO release from PUs in PBS (37 °C, pH 7.41) for (black) RSNO, (green) 3:1 RSNO:DET, (blue) 1:1 RSNO:DET, and (red) DET/NO systems. The inset displays a magnified view of the initial NO-release profile for the DET/NO sample.

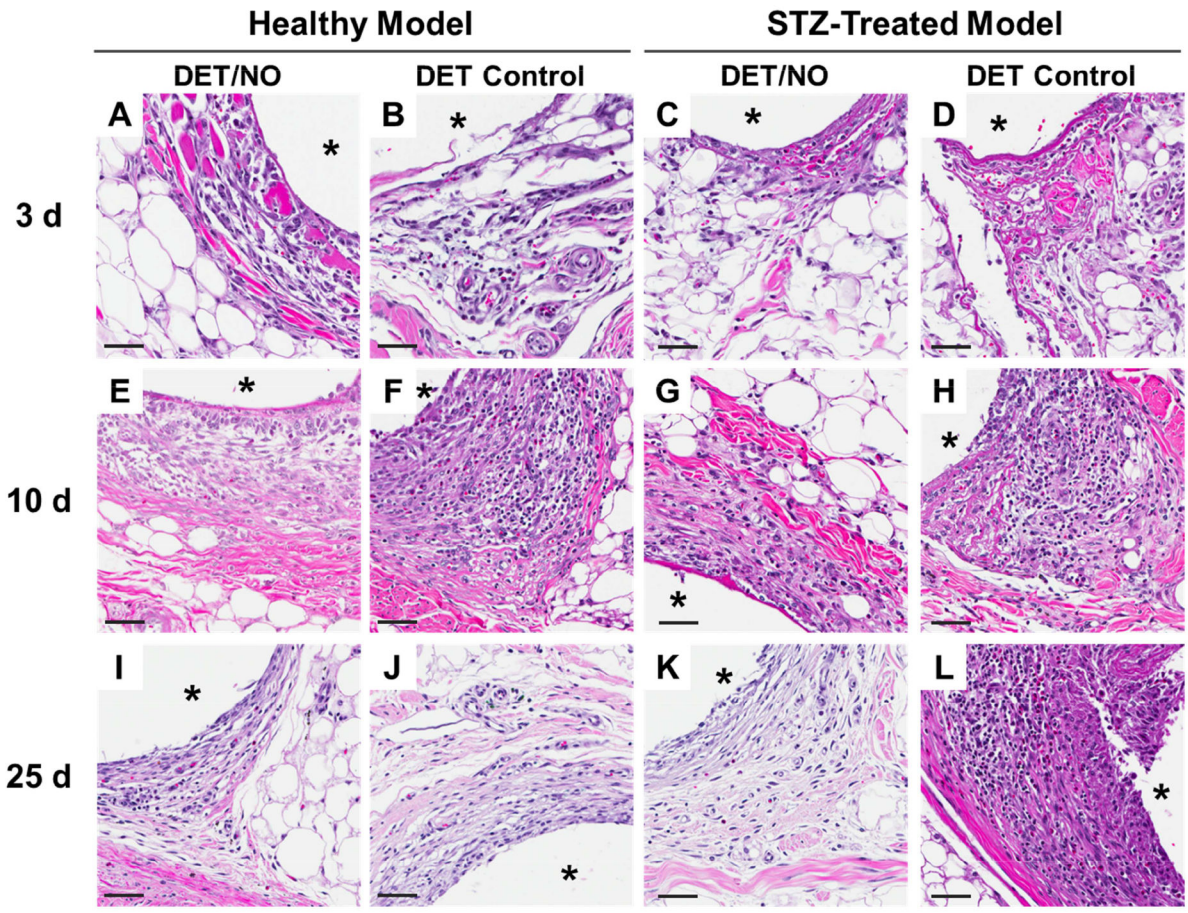

Figure 3.

Photomicrographs of hematoxylin and eosin-stained tissues adjacent to implanted PU materials at (A–D) 3;(E–H) 10; and (I–L) 25 d post-implantation. The number of dark purple inflammatory cell nuclei were quantified as a measure of inflammation severity. The asterisk (*) in each image indicates the location of the implant. The scale bar at the bottom of the image represents a distance of 50 μm. DET/NO and DET Control implants were selected to show large differences in the magnitude of the FBR, which are readily visualized in the H&E images.

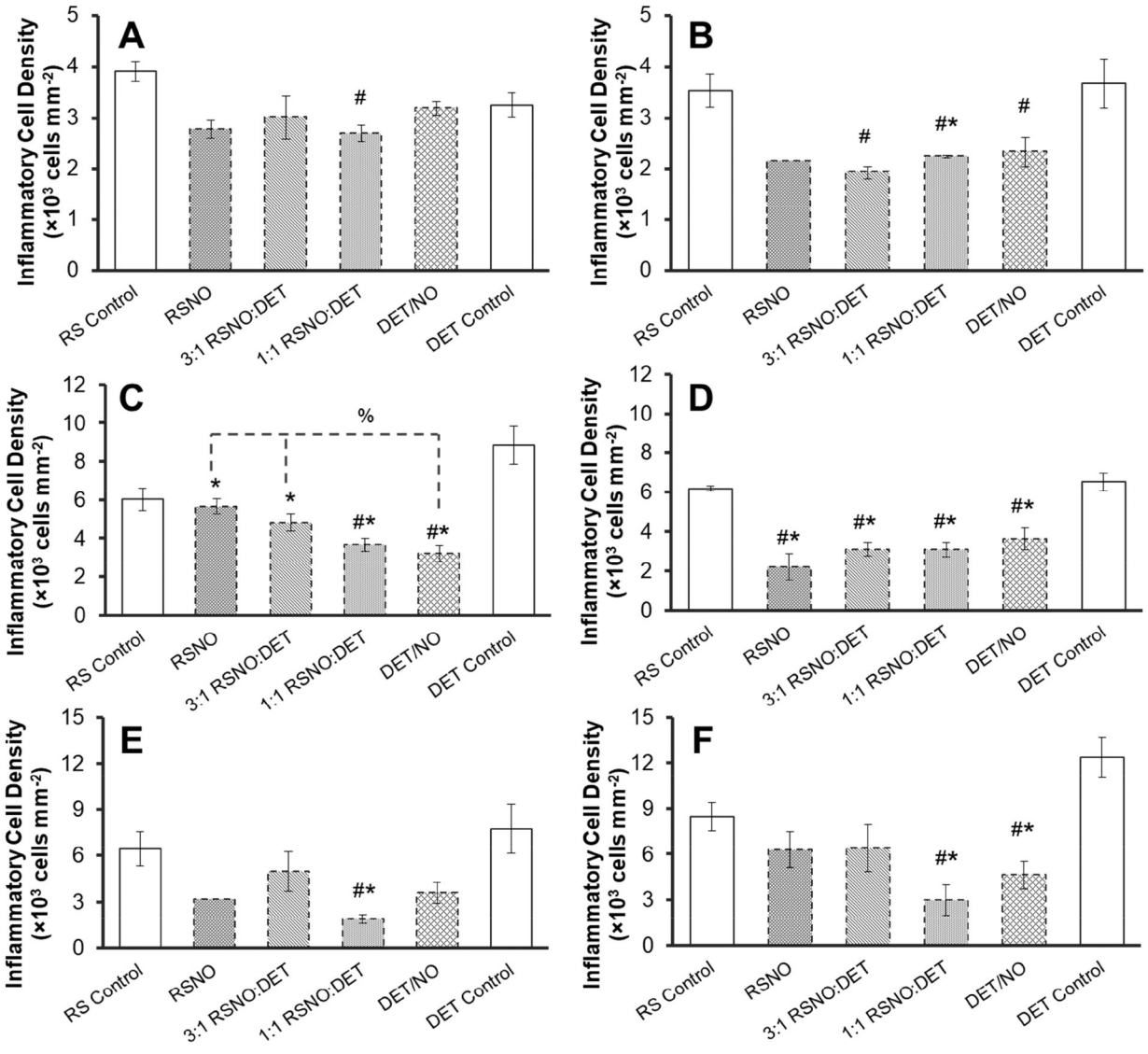

Figure 4.

Inflammatory cell densities in the vicinity of subcutaneously-implanted mock sensors at (A, B) 3; (C, D) 10; and (E, F) 25 d post-implantation in (A, C, E) healthy and (B, D, F) STZ-treated pigs. Inflammatory cell counts are expressed as average densities (±standard error of the mean) within 200×100 μm areas of tissue immediately adjacent to the implants. Symbols above individual bars denote statistical significance between NO-releasing and either DET (*) or RSNO (#) control samples at $p<0.05$. Where appropriate, differences between individual NO-release systems are marked with a % symbol. Statistical testing was not carried out for the RSNO sample in graphs (B) and (E) due to insufficient sample size. For all other samples, results are aggregate data for 3–4 separate implants.

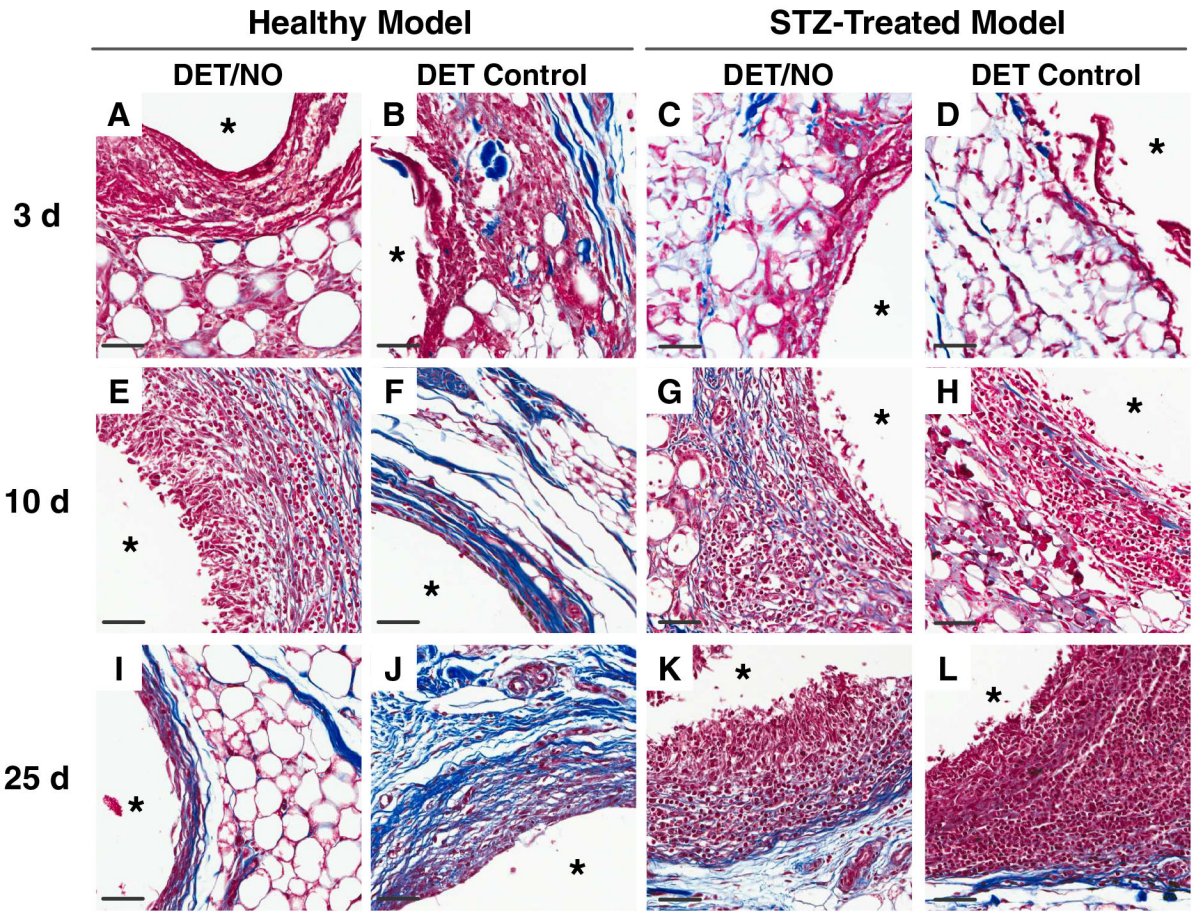

Figure 5.

Representative photomicrographs of Masson's Trichrome-stained tissues adjacent to implanted PU materials at (A–D) 3; (E–H) 10; and (I–L) 25 d post-implantation. Collagen density was analyzed in 200×50 μm areas immediately proximal to the implant surface and expressed as the % area occupied by blue-stained collagen. The asterisk (*) in each image indicates the location of the implant. The scale bar at the bottom of the image represents a distance of 50 μm. DET/NO and DET Control implants were selected to show large differences in the magnitude of the FBR, which are readily visualized in the MT images.

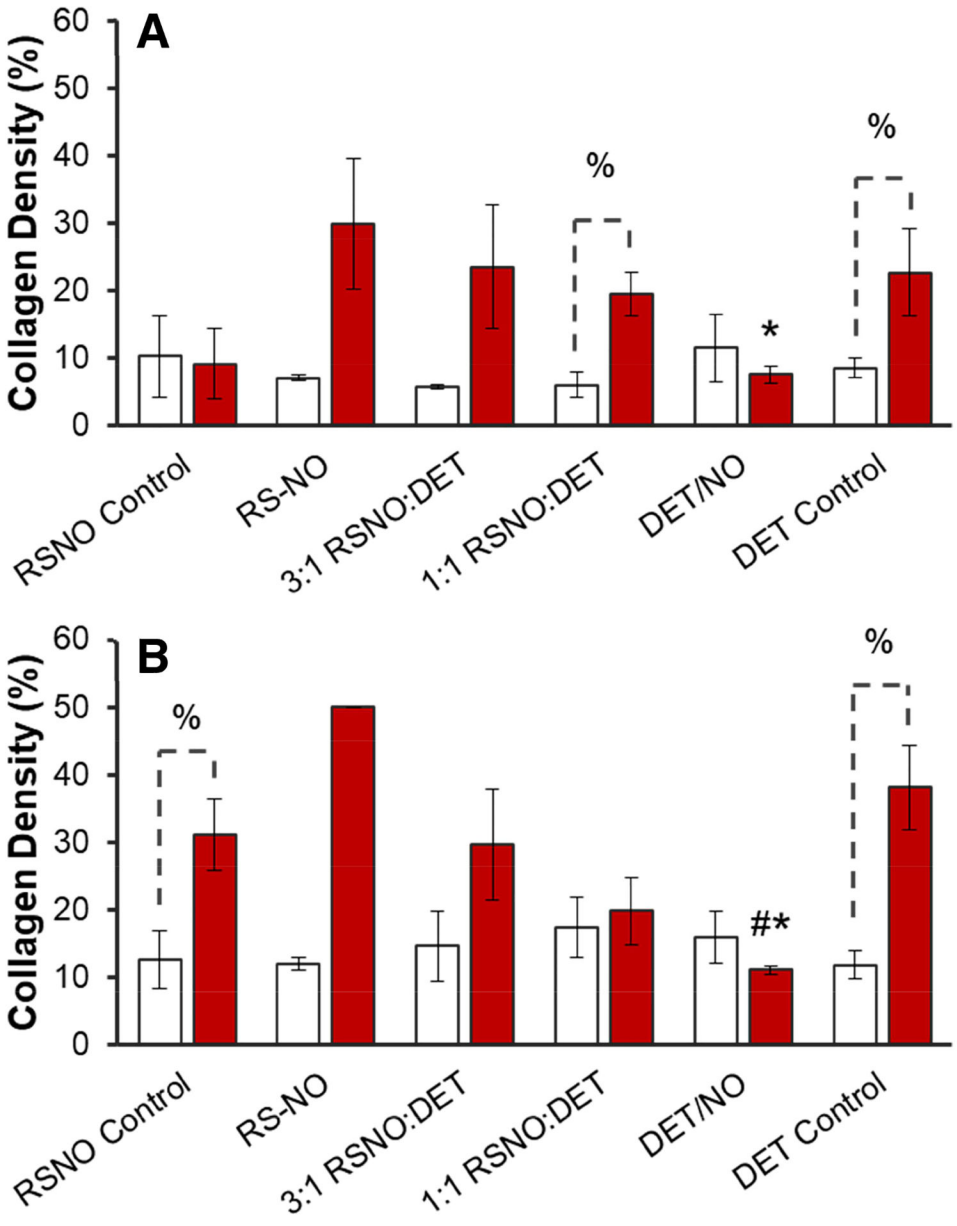

Figure 6.

Collagen densities in the tissue surrounding mock sensors at (A) 10 and (B) 25 d post-implantation for healthy (red bars) and diabetic swine (open bars). Collagen densities are expressed as average values (±standard error of the mean). Symbols above individual bars denote statistical significance between NO-releasing and either DET (*) or RSNO (#) control samples at $p<0.05$. Where appropriate, differences between identical samples implanted in healthy or STZ-treated pigs are denoted with a % symbol. Statistical testing was not carried out for the RSNO sample in (B) due to insufficient sample size. For all other samples, results are aggregate data for 3–4 separate implants.

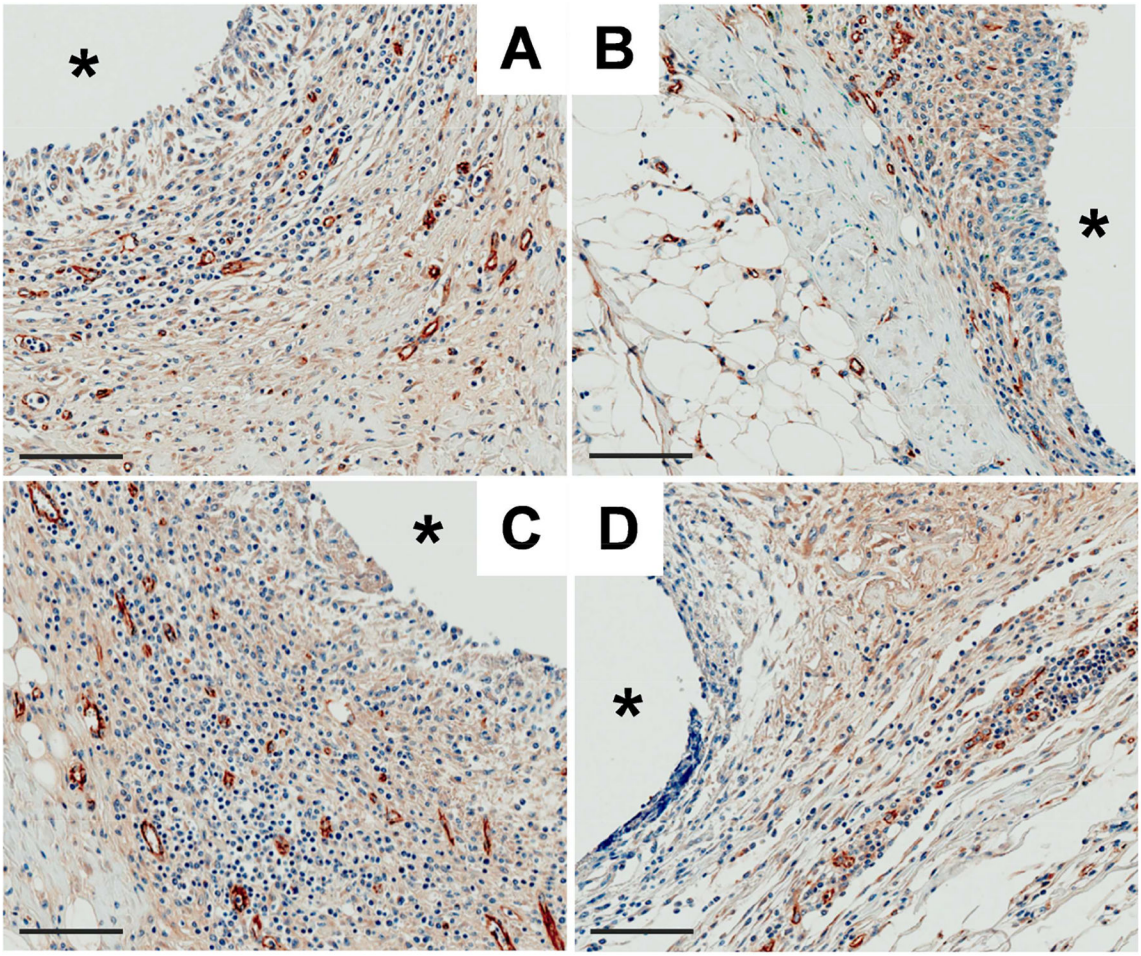

Figure 7.

Photomicrographs of anti-CD31 and hematoxylin stained tissues adjacent to (A, C) DET/NO and (B, D) DET control implants after 10 d in the (A, B) healthy and (C, D) diabetic pigs. Blood vessels were identified as open tubular brown structures. The asterisk (*) marks the implant location and the scale bar at the bottom left of each image represents 100 μm.

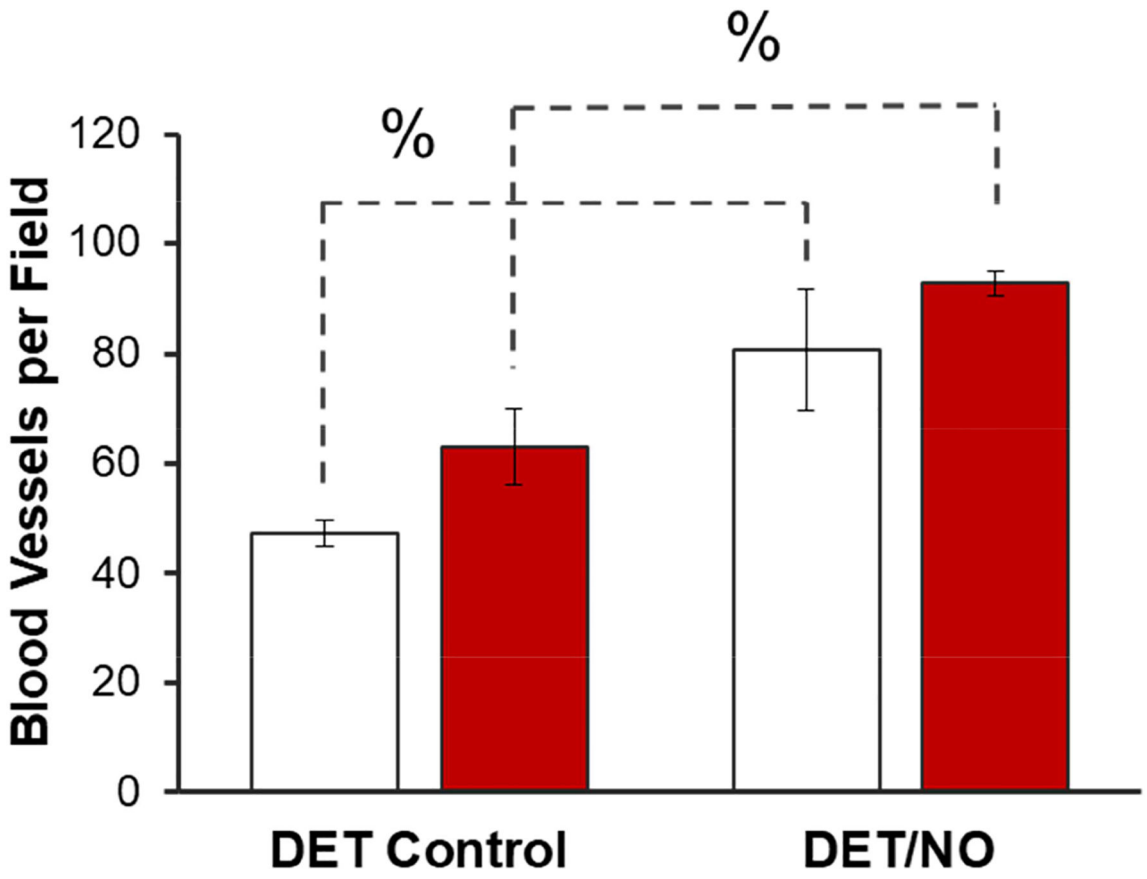

Figure 8.

Blood vessels within 400 μm of the surface of DET/NO and DET control implants 10 d post-implantation in healthy (red bars) and diabetic (open bars) swine. The % symbol denotes a significant difference between two implants at $p<0.05$. Data are presented as aggregate results for n=3 of each implant type.

Table 1.

Nitric oxide release from polyurethane membranes doped with different NO donor-modified silica nanoparticles.[a]

NO-Release System	[NO][b] (pmol cm^{-2} s^{-1})								
	4 h	12 h	24 h	48 h	72 h	96 h	144 h	240 h	312 h
RSNO	18.1±8.9	6.1±2.1	3.2±0.8	0.9±0.1	---	---	---	---	---
3:1 RSNO:DET	23.5±2.9	5.3±1.9	3.8±0.4	1.8±0.7	0.8±0.3	---	---	---	---
1:1 RSNO:DET	54.7±8.5	18.5±2.2	9.7±0.8	8.4±3.6	5.5±1.6	3.3±1.0	2.1±0.5	---	---
DET/NO	8.4±0.7	5.7±0.5	4.1±0.6	3.5±0.4	2.9±0.4	3.2±0.6	2.6±0.5	1.4±0.2	0.8±0.2

[a]Results are expressed as average values ± standard deviation of n>3 separate experiments.

[b]Instantaneous NO flux measured from mock sensor surfaces via chemiluminescence NO analysis.